

# Architecturally modified Al–DRA composites: the effect of size and shape of the DRA rods on fracture behavior

M. Jamali · Kh. Farokhzadeh · R. Bagheri ·  
S. M. Seyed Reihani

Received: 26 September 2009 / Accepted: 25 January 2010 / Published online: 17 February 2010  
© Springer Science+Business Media, LLC 2010

**Abstract** Architectural modification of aluminum matrix composites is considered as an efficient method to improve fracture toughness. Al–DRA (Al–Al/SiC/20<sub>p</sub>) composites were fabricated via “powder extrusion–casting–ingot extrusion” route with structures similar to that of reinforced concrete, so that DRA rods were surrounded by unreinforced aluminum. The effects of variation in shape, size, and number of DRA rods on fracture behavior of Al–DRA composites were investigated. Composites containing DRA rods with hexagonal cross-section exhibited higher resistance to crack initiation and growth, in comparison to those containing circular rods. In the case of hexagonal rods, increasing the number of rods (reducing the rods’ cross-section surface) led to further enhancement of fracture toughness. Fracture surface observations of all samples revealed the existence of desirable cohesion between rods and the surrounding matrix. The remained sharp and unblunted corners of hexagonal DRA rods caused stress concentration and microcrack formation upon loading. Hence, plastic deformation constraint of aluminum ligament between rods was alleviated, which, in turn, led to further energy consumption during the fracture process.

## Introduction

Particulate-reinforced metal matrix composites (MMCs), have received considerable attention due to their desirable physical and mechanical properties such as improved

strength and stiffness, favorable stability at elevated temperatures, good wear resistance and also feasibility for mass production by conventional methods [1–3]. However, inadequate ductility, fracture toughness, and impact energy restrict extensive application of these materials in industry [4–6].

Aluminum alloys are the most widely used matrices in MMCs both in research and development and in industrial applications. This is mainly due to their low density and cost (compared with other low density alloys such as magnesium and titanium), ductility, corrosion resistance, thermal conductivity, and heat treatment capability. Discontinuously reinforced aluminum composites (DRAs) have various applications in industries from automotive and aeronautics to electronics and leisure [7–9].

Since low ductility and fracture toughness are the major drawbacks of using DRAs, in recent years significant efforts have been devoted to investigate fracture mechanisms and methods for improving the fracture toughness in this family of engineering materials [10–17]. In general, these methods can be classified as microstructural and architectural modifications [18] (in the other literature these two methods entitled intrinsic and extrinsic toughening methods, respectively [19–21]). Control and tailoring of microstructural parameters of the composites such as size, volume fraction, and distribution of the reinforcement particles, matrix alloy and the properties of the interface between them are considered in the first technique [22–26]. On the other hand, architectural modification involves introducing ductile regions of aluminum within the more brittle DRA regions in such a way that crack propagation rate in the material is decreased and hence, the impact energy and toughness is increased [20, 27]. This methodology can affect stress state at the crack tip and also activates extrinsic toughening mechanisms such as crack

---

M. Jamali · Kh. Farokhzadeh · R. Bagheri (✉) ·  
S. M. Seyed Reihani  
Department of Materials Science and Engineering, Sharif  
University of Technology, P.O. Box 11155-9466, Tehran, Iran  
e-mail: rezabagh@sharif.edu

deflection, bridging, trapping, and shielding, in addition to intrinsic ones [20, 21, 27].

Among various approaches considered for architectural modification of these composites are fabrication of layered composites [15, 16, 18, 19, 28–31], functionally graded materials [32, 33], and reinforced concrete-like structure composites [34–36]. Pandey et al. [18] exploited the higher apparent toughness of thin DRA lamina to obtain a laminate of higher thickness and toughness. Compared to the monolithic DRA, the composite consisting of alternate layers of DRA and unreinforced aluminum alloy showed considerable toughness improvements. Wu et al. [31] have also reported excellent fracture toughness in the crack arrester orientation of layered Al6061–Al6061/SiC<sub>p</sub> composites that were fabricated by spray deposition. Nardone et al. [34] incorporated continuous ductile toughening tubular regions throughout the composite to improve damage tolerance. In another research by Qin and Zhang [36], designed and fabricated Al6061–Al6061/SiC<sub>p</sub> composite with architecture similar to reinforced concrete showed significant increase in fracture toughness compared to the conventional composites. Unlike conventional aluminum composites, in the modified composite catastrophic fracture did not occur upon loading, and the fracture took place in several stages; thus, more energy was consumed [36]. The plastic deformation of Al ligament, between the reinforcing DRA rods, at the crack front was known responsible for enhanced energy absorption and hindering of rapid crack propagation [36].

In order to improve the fracture toughness of DRAs while retaining their mechanical strength, several investigations have been performed in this group to design and fabricate Al–DRA composites. While casting [5, 17] and powder metallurgy [6, 9, 12] are widely used to produce aluminum matrix composites; a combination of powder extrusion and casting routes was utilized in this group to fabricate Al–DRA composites with architecture similar to that of reinforced concrete [37, 38]. Following the previous findings, in the current study the effect of variation in shape, size, and number of DRA rods—and thus the morphology of the reinforcing rods/matrix interface—in

improving the fracture toughness of the designed composites is investigated.

## Experimental procedure

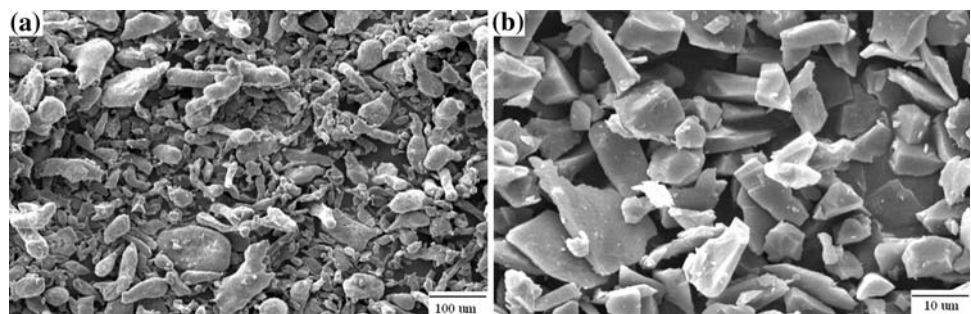
Al/SiC<sub>p</sub> composites (DRAs) were produced by powder extrusion. Commercially pure aluminum powder, i.e., Al 99.41 and (Si + Fe) 0.43 wt%, with an average size of 63 μm was used, and the composites were reinforced with 20 vol.% of SiC particles with an average size of 18 μm (Fig. 1).

The metal and ceramic powders were mixed in a Turbula mixer for 40 min. Mixed powders were then cold pressed in aluminum cylindrical cans with a diameter and height of 136 and 185 mm, respectively, under a constant pressure of 65 MPa. The cans were then heated to 460 °C for 40 min and finally hot extruded at 440 °C into rods with three different cross-sections: two hexagons with side sizes of 6.2 and 9.1 mm (extrusion ratio of 42:1) and a circle with a diameter of 18.2 mm (extrusion ratio of 18:1). The ram speed was about 1 mm/s and a graphite based lubricant was used.

DRA rods were then placed into steel dies. The dies and DRA rods were preheated at 250 °C before pure aluminum melt was degassed and poured into the dies at 700 °C. Ingots of 150 mm diameter and 180 mm height were obtained which were then hot extruded at 400 °C into rectangular bars (25 × 34 mm) with extrusion ratio of 21:1. Ram speed and lubricant used were the same as above. Figure 2 schematically illustrates the fabrication route used in the present work to obtain Al–DRA composites. Specifications of the fabricated Al–DRA composites are presented in Table 1.

Polished surfaces from the cross-section of DRA samples (perpendicular to the extrusion direction) were examined by means of an optical microscope (OLYMPUS BX51). Density of each sample was carefully evaluated via Archimedes technique; consequently, the relative density of samples was calculated by dividing of measured density to the theoretical one. Sub-sized cylindrical tensile samples

**Fig. 1** Scanning electron micrographs of **a** aluminum powder and **b** SiC powder used in this work



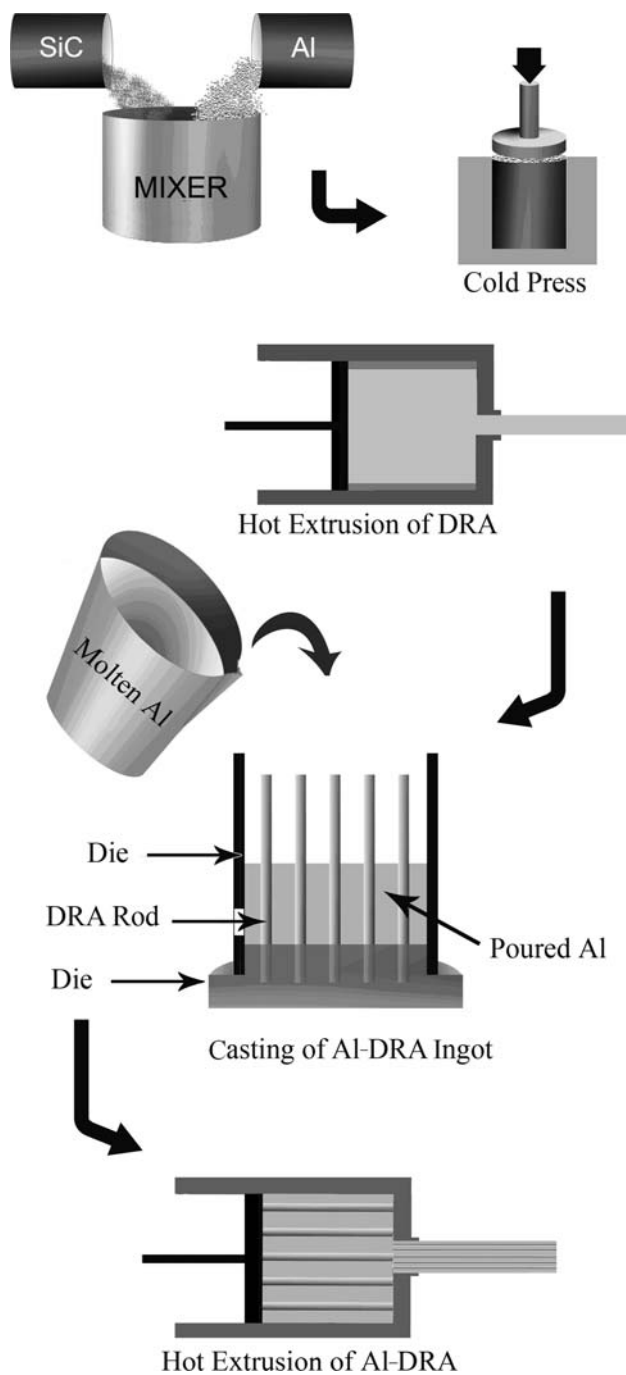


**Fig. 2** Schematic illustration of the procedure used to obtain Al-DRA composites

were prepared from monolithic DRA and Al extrudates with gauge length and diameter of 30 and 6 mm, respectively. Tensile test was then performed on the specimens according to ASTM E8m [39], using a Hounsfield H10KS universal frame. Fracture toughness of Al-DRA composites was evaluated on three-point bend specimens in the crack arrestor orientation (crack growing perpendicular to the direction of reinforcing DRA rods), in accordance with the ASTM E399 [40] and ASTM E992 [41]. The test was

**Table 1** Specifications of fabricated Al-DRA composites

Sample's code	Number of DRA rods	DRA cross-section	Total volume fraction of SiC <sub>p</sub> in the composite
H-19	19	Hexagon ( $a = 9.1$ mm)	6.2
C-19	19	Circle ( $D = 18.2$ mm)	5.5
H-37	37	Hexagon ( $a = 6.2$ mm)	6.1

carried out on  $32.1 \times 23.1 \times 156$  mm specimens, and due to the difficulties encountered in generating uniform fatigue-induced initial cracks in these composites, all samples were notched via EDM. The tests were carried out using an Instron 8502 servo hydraulic frame under cross-head speed of 1 mm/min. Finally, the fracture surfaces of specimens were analyzed under a scanning electron microscope (PHILIPS XL30) and a stereo microscope (OLYMPUS SZH10).

## Results and discussion

### Mechanical properties of aluminum and DRAs

Uniaxial tensile test results indicate that introducing ceramic particles to the aluminum matrix results in a rise in strength and elastic modulus and a significant decline in ductility. As illustrated in Fig. 3, the unreinforced aluminum shows a total engineering strain around 30%, while the composite reinforced with 20 vol.% of SiC particles cannot endure more than 7% of engineering strain. On the other hand, elastic modulus of aluminum increases from 69 to 105 GPa by introducing 20 vol.% of SiC particles.

Several mechanisms are known to be responsible for this strengthening effect, the two most important ones are as

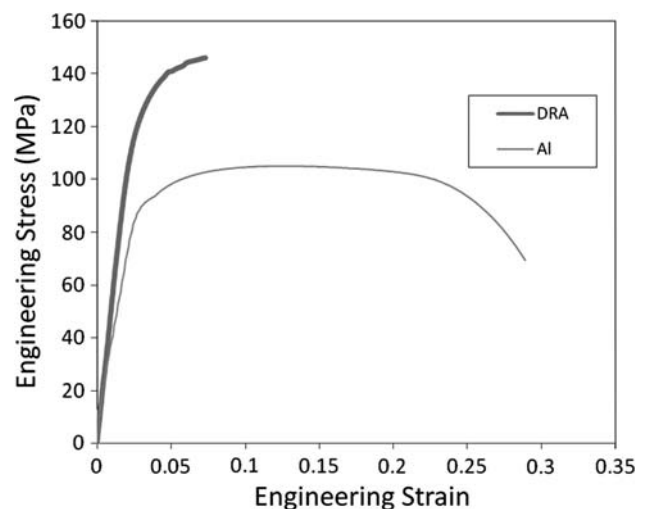


**Fig. 3** Tension test results for Al and DRA

follows. (1) Modified Shear Lag (MSL) model based on the shear lag theory, proposed by Nardone and Prewo [42], attributing the strengthening behavior to higher load bearing capacity of ceramic particles. The difference in elastic modulus of aluminum and SiC (69 and 430 GPa for aluminum and SiC, respectively [43]) causes a non-uniform distribution of load in the two phases; hence, the ceramic particles endure a greater amount of stress. Therefore, the matrix experiences a lower local stress than the nominal applied stress, and the material yields under larger applied stress conditions [42, 44]. (2) The Enhanced Dislocation Density (EDD) theory attributed the strengthening mainly to the enhanced strength of the matrix due to the increase in dislocation density. The increase in dislocation density is assumed to be a simultaneous action of the dramatic difference in the coefficient of thermal expansions and the mismatch in elastic modulus of the reinforcement phase and the matrix that result in the formation of geometrically necessary dislocations [45, 46]. Composite's strength increases while its plastic deformability decreases with increasing dislocation density [45, 46].

The non-uniform distribution of reinforcing particulates in the matrix results in early fracture of the composite. Therefore, powder metallurgy was utilized to fabricate DRAs in the current research because compared to liquid-phase processes; it has the advantage of yielding a more

appropriate distribution of reinforcement particles. Figure 4 shows that SiC particles are well distributed in the aluminum matrix almost without any agglomeration.

For precise evaluation of the porosity content, density measurements were performed. As tabulated in Table 2, the maximum porosity content for the composites is 2.2% while that of the unreinforced aluminum is 0.4%. The higher amount of voids in DRA composites appears to be the result of the presence of the SiC particulates. Indeed, during pressing and extrusion, aluminum particles tend to deform and rearrange themselves to fill the voids between the particles; however, the rigid SiC particulates not only do not deform but also inhibit their surrounding matrix from plastic deformation resulting in non-filled cavities [44]. Figure 5 presents fracture surfaces of tensile specimens for unreinforced aluminum and one of the DRA samples. Microvoid coalescence seems to be the dominant fracture mechanism in both specimens; however, it is significant to note that the size and depth of voids differ in the samples. Ceramic particulates provide more suitable sites for microvoid nucleation and since the aluminum ligament between the particles can only endure limited amount of plastic deformation, the voids cannot grow as much and therefore, dimples on DRA fracture surface are smaller and shallower. SiC particulates are detected in some dimples suggesting that microvoid nucleation has originated from debonding at the interface of aluminum matrix and SiC particles.

To sum up, there is a considerable difference in mechanical properties of Al and DRA materials produced in current research and DRAs exhibit superior strength and inferior ductility to Al. It is noteworthy that observed difference between the two materials is affected by the nature of loading mode, i.e., tensile. Earlier works have revealed that both of Al and DRA behave ductile under compression or superimposed pressure [14, 47].

In previous works regarding fabrication of architecturally modified Al–DRA composites for obtaining enhanced fracture toughness [36, 37], 6xxx series of Al alloys, which are stronger and less ductile than 1xxx series, were used. Therefore, DRA and Al matrix in those researches were considerably stronger and more brittle than the materials used in the present research. However, since the important feature in the efficiency of architectural modification is the

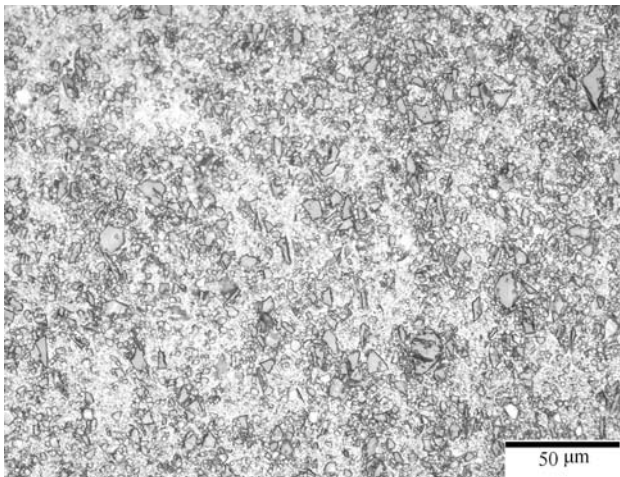
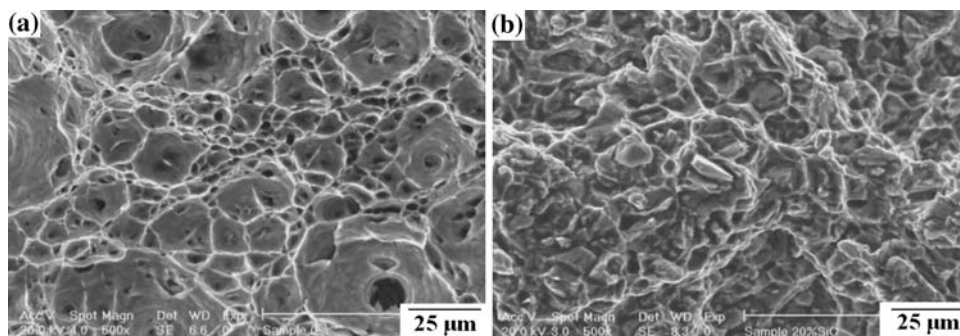


**Fig. 4** Particle dispersion in DRA

**Table 2** Results of density measurement and calculated porosity content

Sample's cross-section	Chemical composition	Extrusion ratio	Measured density	Relative density (%)	Porosity content (%)
Hexagon ( $a = 9.1$ mm)	Al–20%SiC	42	2.74	98.2	1.8
Hexagon ( $a = 6.2$ mm)	Al–20%SiC	42	2.73	97.8	2.2
Circle ( $D = 18.2$ mm)	Al–20%SiC	18	2.74	98.2	1.8
Hexagon ( $a = 9.1$ mm)	Al	42	2.69	99.6	0.4

**Fig. 5** Fracture surface of **a** Al and **b** DRA



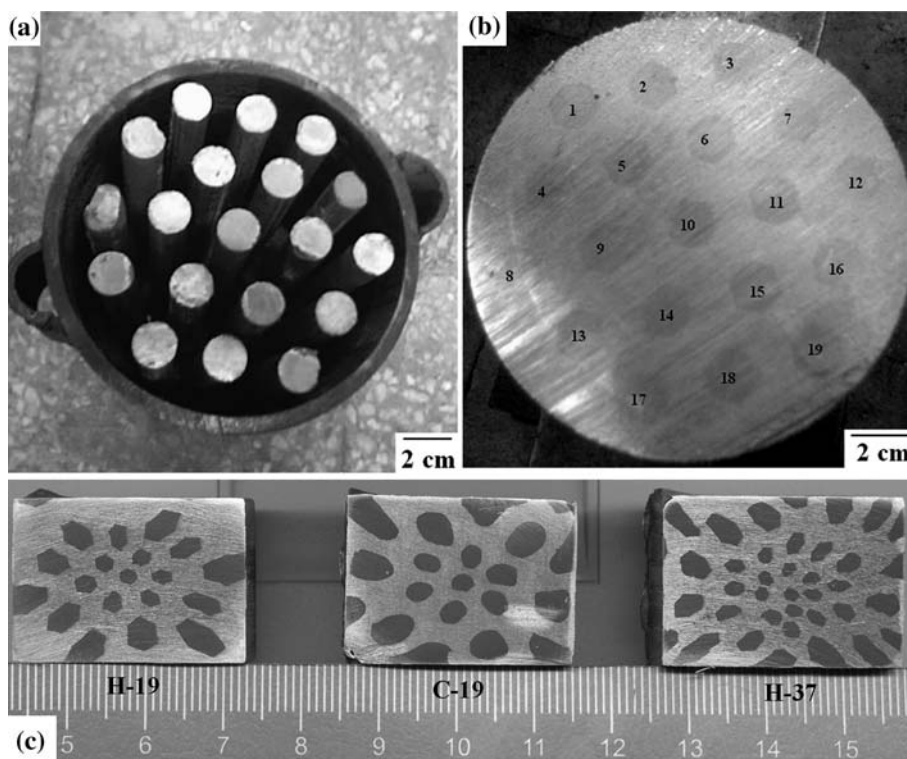
elastic modulus and strength difference between Al and DRA [48], use of 1xxx series in the current study seems logical and fabricated Al–DRA composite can be considered as a model-material to evaluate the effect of size and shape of DRA rods on toughness and fracture behavior of architecturally modified composites.

The structure and morphology of Al–DRA composites

Figure 6 illustrates the configuration of DRA rods in Al–DRA composites during different stages of fabrication. As apparent from Fig. 6a and b, in all composites, rods were initially arranged within equal distances in a defined configuration (hexagonal symmetry). As mentioned before, DRA rods with both circular and hexagonal cross-sections, designated by “C” and “H”, respectively, were made in

this study (The designation used for Al–DRA samples made in this study contains a letter, i.e., “C” or “H”, followed by a number indicating the number of DRA rods located within the Al matrix). Since using circular rods leads to uneven distribution of Al ligament thickness between the rods, DRA rods with hexagonal cross-section were chosen and arranged with parallel adjacent sides to obtain even distribution (Fig. 6b). Figure 6c illustrates non-uniform deformation and arrangement of DRA rods within the composites after extrusion. As one can see, the rods located in the central part of extrudates experienced larger deformation (higher cross-section reduction), but maintained their original shape to a large extent. However, the rods located farther have undergone a non-uniform deformation and are rather extended towards the corners and distorted into non-symmetrical configuration, which is

**Fig. 6** Morphology of Al–DRA composites: **a** C-19 before aluminum melt pouring, **b** H-19 after aluminum melt pouring, **c** Al–DRA extrudates



because of non-uniform stress state in extruding of circular cross-section to the rectangular one. Also it should be noted that the surface of Al–DRA composites was machined prior to three-point bending specimen preparation because they suffered from a small amount of fir-tree defect.

Fracture behavior of Al–DRA composites

Fracture toughness evaluation

Three-point bending test was performed on Al–DRA composites to investigate their fracture behavior. The resulted corresponding Load–Load Point Displacement (Load–LPD) curves are presented in Fig. 7. Upon increasing the applied load, specimens exhibited resistance to crack initiation by elastically bending followed by a small amount of plastic deformation. Further increase in applied load resulted in crack initiation; since, the energy required to continue plastic deformation exceeded the energy required for crack initiation. At this point the maximum peak load in the Load–LPD curve is reached and as the crack starts to propagate, the load declines gradually. As Fig. 7 suggests, H-37 has endured a greater amount in peak load and thus, a higher resistance to crack initiation, while the maximum load sustained for H-19 and C-19 is almost the same. Moreover, the curves for H-37 and C-19 follow more or less the same trend and are nearly parallel to each other; however, in the case of H-19, there is a prolonged range for maximum load and the decrease in load occurs more gracefully in this composite after the peak load is reached.

The area under Load–LPD curve in fracture toughness testing gives a good estimate of the amount of work per unit volume which can be done on the material prior to its rupture which is equal to the energy consumed during this

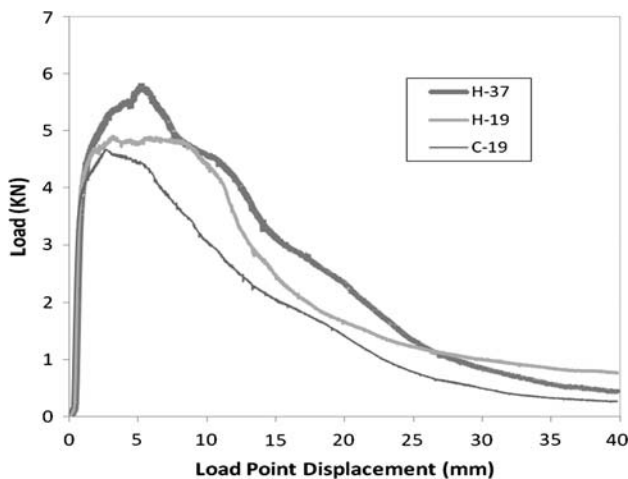


Fig. 7 Load–Load Point Displacement (Load–LPD) curves of architecturally modified composites

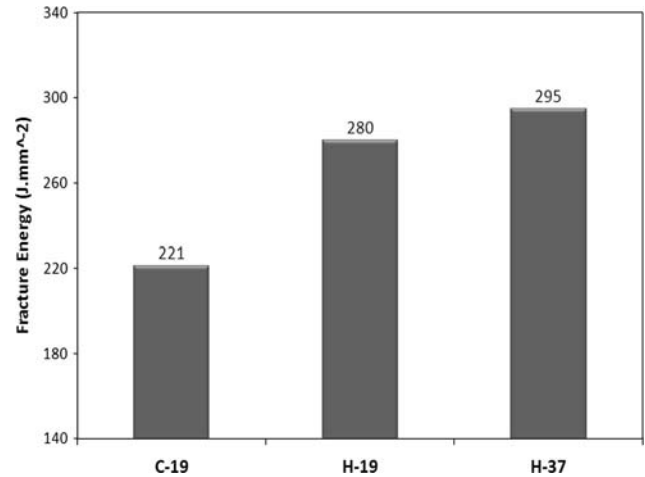


Fig. 8 Normalized area under Load–LPD curves

process [18]. However, due to differences in specimen size, the un-notched areas of different samples have different sizes. Therefore, a normalization process was employed to correct the results and make a valid comparison possible. To normalize the data, calculated area under Load–LPD curve of each sample was divided by its fracture surface area. Normalized results are presented in Fig. 8. According to this figure, H-37 has the greatest normalized area under Load–LPD curve and the largest absorbed energy during its fracture process while that of C-19 was the least.

The fracture toughness ( $K_{IC}$ ) determined in accordance with ASTM E399 [40] is based on the linear elastic fracture mechanics and must meet specified validity criteria. Considering the high deformability of the composites fabricated in this work, test results indicated that the above-mentioned standard could not lead to valid data and therefore, ASTM E992 [41] was incorporated. The test procedure and methodology of the two standards are the same but equivalent energy fracture toughness ( $K_{ec}$ ) which is an indication of the crack extension resistance is determined in the latter practice. This standard was previously practiced for several studies on laminated Al–DRA composites [49]. Figure 9 illustrates the values of  $K_{ec}$  for the fabricated composites. Comparing Figs. 8 and 9 shows similar trends for the absorbed energy prior to fracture and  $K_{ec}$ . H-37 exhibited the largest  $K_{ec}$ , and reducing the number of reinforcing DRA rods to 19 resulted in a lower  $K_{ec}$ , while changing their cross-section from hexagonal to circular yielded a further decrease in  $K_{ec}$ . In order to explain the observed behavior, fracture surface of the bending specimens were examined.

Microscopic features

Macroscopic and microscopic examination of the fracture surfaces give some insight into the responsible mechanisms

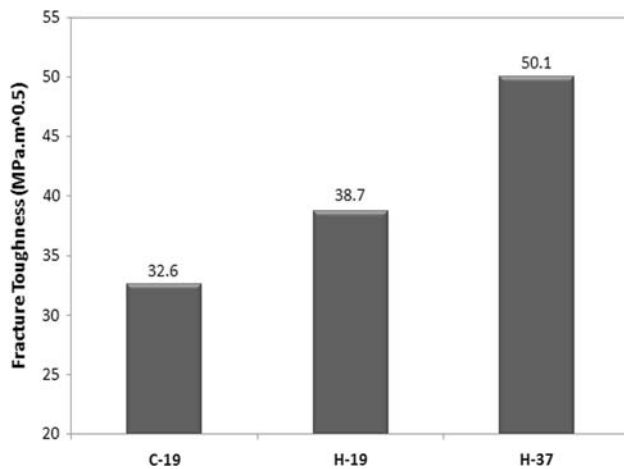


**Fig. 9** Equivalent energy fracture toughness ( $K_{Ic}$ ) of Al-DRA composites

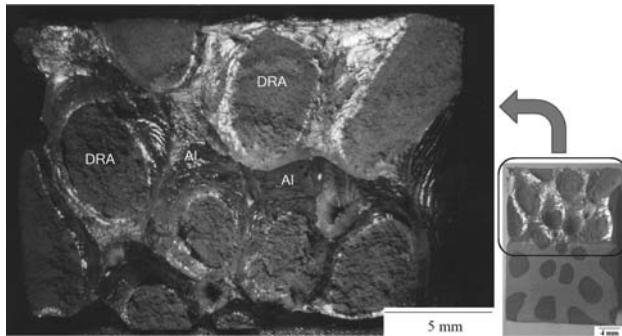


**Fig. 10** Micrograph showing the fracture surface of composite C-19

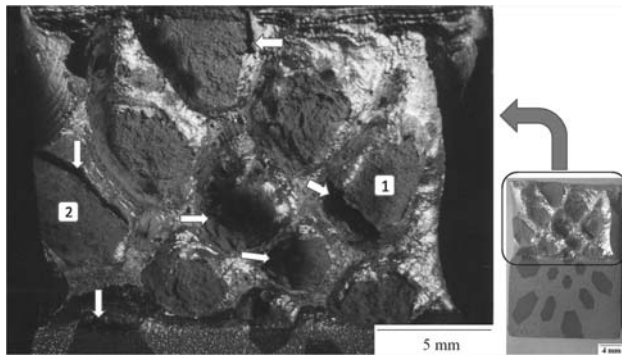


**Fig. 11** Micrograph showing the fracture surface of composite H-19

involved in their fracture behavior. Stereo micrographs of Al-DRA fracture surfaces are illustrated in Figs. 10, 11, and 12. While DRA rods have a fibrous, gray, and uneven fracture appearance, fracture surface of the metallic matrix appears bright and luminous with necked regions suggesting extensive shear deformation prior to the final failure. As for the C-19 composite, all DRA rods have remained in conjunction with the matrix with no evidence of interfacial debonding (Fig. 10); however, microcracks

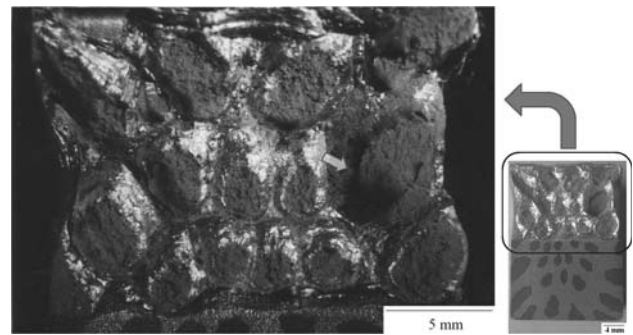


**Fig. 12** Micrograph showing the fracture surface of composite H-37

have been observed at several regions near Al/DRA interface in H-19 (Fig. 11). For example, in the DRA labeled as (1) in Fig. 11, the microcrack has nucleated and totally propagated within the DRA region until the crack front reaches the aluminum ligament, where it stops and finally the DRA is divided into two sections (cohesive failure). The same scenario is observed for all cracked DRAs except for the DRA labeled as (2); in which interfacial debonding has occurred (adhesive failure). A sharp corner of the rod has touched the peripheral side of specimen—caused by removing the outer part of aluminum ligament during machining—and therefore, stress concentration has resulted in crack nucleation at the interface and growth along it till debonding has occurred.

Generally it could be said that aluminum and DRA are well-bonded (as illustrated in Fig. 13) which is expected considering the same alloy used in the ligament and matrix of DRA rods and the extensive shear deformation during the extrusion process.

In spite of having hexagonal DRA rods, fracture surface of H-37 significantly differs from that of H-19. There are no microcracks or interfacial debonding present in the fracture surface of H-37 (Fig. 12) excluding the one DRA

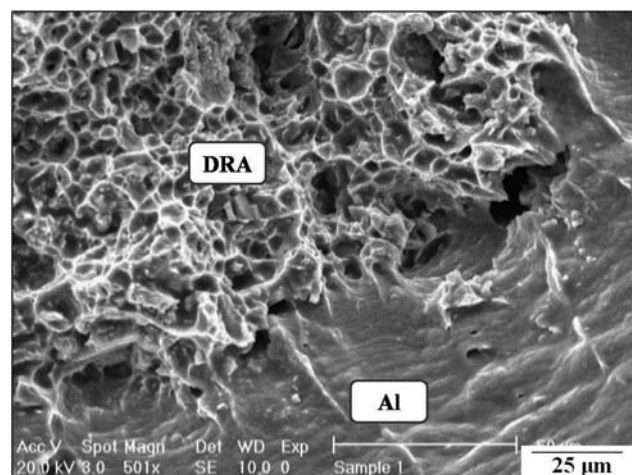


**Fig. 13** Well-bonded interface of Al and DRA in microscopic scale

indicated by arrow, in which a microcrack has initiated close to the interface and spread across the rod. This behavior can be explained referring to Fig. 6. As mentioned earlier, extensive plastic deformation during extrusion has led to smaller DRAs at the center with blunt corners and larger DRAs maintaining their sharp corners at margins. Due to the difference in elastic modulus and strength of aluminum and DRA, upon loading, these sharp corners lead to stress concentration and microcrack formation in the more brittle phase (DRA).

Initial cross-section of a DRA rod in H-19 was almost 2 times of that in H-37. Moreover, blunting of the corners during extrusion took place in the larger DRAs less often than smaller ones. Hence, there were more stress concentration zones in the H-19 than H-37 and many of DRA rods in H-19 have broken. SEM micrograph from the H-19 fracture surface also confirms the probability of microcrack initiation from the hexagon's corner and its growth inside the rod (Fig. 14).

In architecturally modified composites (e.g., laminated or with reinforced concrete design) in which the two components possess different mechanical properties, the presence of the stiffer component (DRA) and a well-bonded interface, constrain plastic deformation of the more ductile phase (aluminum) and result in large stress triaxiality (tensile hydrostatic stress) in the matrix [48]. This constraint is directly proportional to the difference in elastic modulus and yield strength of the components [48]. Comparing dimple size in aluminum ligament in H-37 (Fig. 15) and un-reinforced aluminum (Fig. 5a) reveals an increase in hydrostatic stress field at the crack tip. According to the Rice and Tracey model [50], the dimple growth rate is directly proportional to the hydrostatic stress level and thus dimple size in the aluminum ligament under

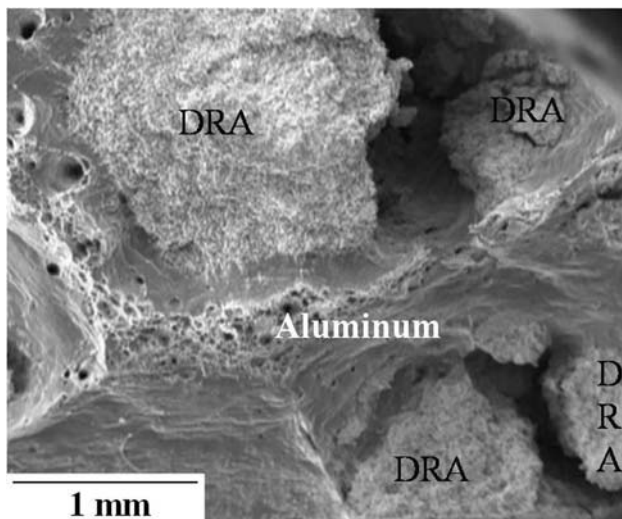


**Fig. 14** SEM micrograph of broken DRAs in composite H-19

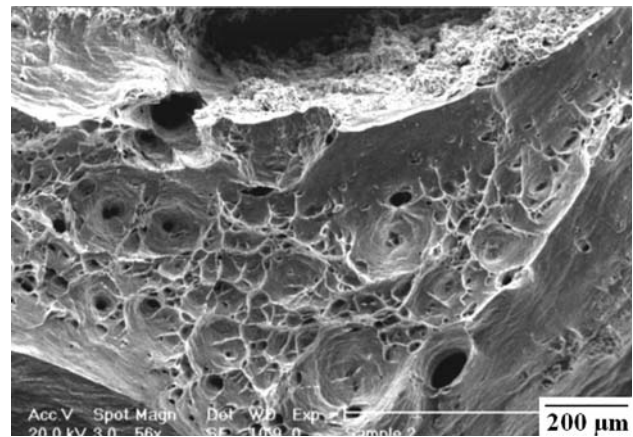


**Fig. 15** Dimples of aluminum ligament in composite H-37

constraint is found to be larger. Although, other works where hydrostatic compressive stresses have been superimposed have conversely shown that such stress states inhibit damage initiation and accumulation while reducing the dimple size [14, 47].

The thinner the Al ligament, the larger the deformation constraint. In order to reduce or relax the constraint and facilitate ligament's deformation, the system may respond by interfacial debonding, microcrack formation, or plastic deformation in DRA [48, 49]. As stated earlier, no interfacial debonding was observed in the specimens, which suggests that the DRAs have been initially deformed and work hardened and then microcracks have formed under more severe stress concentration conditions. Since H-37 has had the thinnest aluminum ligament among its reinforcing rods, it has possessed the largest deformation constraint and needed higher levels of applied stress for bending, which is in agreement with Load–LPD curves (Fig. 7). The trend in Load–LPD curve of C-19 is very similar to that of H-37, but occurs at a lower load level. This could be firstly attributed to the larger distance between the DRA rods and lower constraint of the metallic matrix between them and secondly in both composites neither interfacial debonding nor microcracks have been observed. In fact, upon loading these composites, the aluminum ligaments' yielding has been delayed and they have experienced a less amount of plastic deformation, compared to those under unconstrained condition.

The failure process looks slightly more complicated for H-19. In that on one hand the aluminum ligament has been under constraint for plastic deformation and on the other hand, sharp corners present in the hexagonal cross-section have enhanced stress concentration (Fig. 11). As a result, microcracks have nucleated and propagated in DRAs to decrease the constraint in adjacent ligament. Cracking in two neighboring DRAs result in unconstrained deformation of the ligament in between, more strain energy absorption

and enhanced resistance to fracture. It should be noted that cracking does not occur simultaneously in the whole cross-section. With the propagation of the main crack, stress condition at the crack front reaches a critical level and DRAs close to the crack front develop microcracks and the metallic matrix undergoes considerable plastic deformation. This results in a Load–LPD curve with maximum point extending over a range of displacements rather than a single extremum (Fig. 7).

Since the composites fabricated in this research were investigated as model-materials, it can be expected that using high-strength aluminum alloys, H-37 would be the best configuration due to the largest deformation constraint and better resistance to fracture. High-strength aluminum alloys have lesser amounts of plastic deformability; therefore, debonding at Al–DRA interface may also take place that facilitates plastic deformation of Al ligaments and increases energy absorption during failure and thus inhibits catastrophic failure. Also, obtaining higher fracture toughness values seems expectable by using hexagonal-cross-sectioned DRAs with blunted corners.

## Conclusions

Architecturally modified Al–DRA composites with a reinforced concrete design were fabricated via powder extrusion–casting–ingot extrusion route. In order to investigate the effect of shape and size of reinforcing rods on the fracture toughness and behavior of the composites, hexagonal and circular rods were incorporated. The results of the present study are as follows:

1. Tensile test results indicated that the difference between elastic modulus and strength of Al and those of DRA materials used in this study were sufficient to be used as model-materials in investigating the fracture behavior of the designed composites.
2.  $K_{ee}$  values and normalized surface area under the Load–LPD curves of the composites indicated a similar trend such that H-37 showed the maximum amount of energy absorption in fracture while the resistance to fracture was the least in C-19.
3. In the case of H-37 and C-19 composites almost no interfacial debonding or microcracks were observed in the fracture surface of reinforcing DRA rods. Due to the close arrangement of DRA rods in H-37, plastic deformation of the aluminum ligament has been highly constrained and thus, the composite has endured higher stress levels prior to its final failure.
4. Sharp corners of DRA rods in H-19 led to stress concentration and microcrack formation in them which consequently resulted in reduced deformation constraint in the aluminum matrix surrounding reinforcement rods and enhanced resistance to crack propagation.
5. It appeared that using DRA rods with a hexagonal cross section and having an even distribution of ligament thickness between the reinforcing phases can lead to improved fracture toughness of the composites. Blunting the sharp corners of hexagons is also expected to increase the fracture resistance.

## References

1. Nishida Y (2004) In: Cantor B, Dunne FPE, Stone IC (eds) Metal and ceramic matrix composites. Institute of Physics, Bristol
2. Kaczmar JW, Pietrzak K, Wloinski W (2000) *J Mater Proc Technol* 106:58
3. Kim JW (2008) *Mater Sci Eng A* 383–384:648
4. Miracle DB (2005) *Compos Sci Technol* 65:2526
5. Qian L, Kobayashi T, Toda H, Wang Z (2001) *Mater Sci Eng A* 318:189
6. Slipenyuk A, Kuprin V, Milman Y, Gonchanruk V, Eckert J (2006) *Acta Mater* 54:157
7. Downes TJ, King JE (1993) *Composites* 24:276
8. Gnjidić Ž, Grbovic J, Mitkov M, Božić D (2003) *Powder Metall* 46:21
9. Torralba JM, Costa CE, Valesco F (2003) *J Mater Proc Technol* 133:203
10. Ferry M, Monroe PR (2003) *Mater Sci Eng A* 358:142
11. Hu GK, Guo G, Baptiste D (1998) *Comput Mater Sci* 9:420
12. Jain MK, Bhanuprasad VV, Kamatt SV, Pandey AB, Varma VK, Bhat BV, Mahajan YR (1993) *Int J Powder Metall* 29:267
13. Lloyd DJ (1994) *Int Mater Rev* 39:1
14. Liu DS, Lewandowski JJ (1993) *Metall Mater Trans A* 24:609
15. Ellis LY, Lewandowski JJ (1994) *Mater Sci Eng A* 183:59
16. Manoharan M, Ellis LY, Lewandowski JJ (1990) *Scr Metall Mater* 24:1515
17. Rozak G, Lewandowski JJ, Wallace JF, Altmisoglu A (1992) *J Compos Mater* 26:2076
18. Pandey AB, Majumdar BS, Miracle DB (2001) *Acta Mater* 49:405
19. Xu Q, Hayes RW, Hunt WH Jr, Lavernia EJ (1999) *Acta Mater* 47:43
20. Irfan MA, Prakash P (2000) *Int J Solids Struct* 37:4477
21. Lesuer DR, Syn CK, Sherby OD, Wadsworth J, Lewandowski JJ, Hunt WH Jr (1996) *Int Mater Rev* 41:169
22. Agrawal P, Sun CT (2004) *Compos Sci Technol* 64:1167
23. Cocen U, Onel K (2002) *Compos Sci Technol* 62:275
24. Miserez A, Mortenson A (2004) *Acta Mater* 52:5331
25. Zhao Z, Zhihian S, Yingkun X (1991) *Mater Sci Eng A* 132:83
26. Vaidya A, Lewandowski JJ (1996) *Mater Sci Eng A* 220:85
27. Manoharan M, Lewandowski JJ (1990) *Acta Metall Mater* 39:489
28. Biner SB (2001) *J Mater Sci* 36:2505. doi: [10.1023/A:1017942418047s](https://doi.org/10.1023/A:1017942418047s)
29. Osman TM, Hassan HA, Lewandowski JJ (2008) *Metall Mater Trans A* 39:1993
30. Osman TM, Lewandowski JJ (1994) *Scr Metall Mater* 31:191
31. Wu M, Zhang J, Hunt WH Jr, Lewandowski JJ, Lavernia EJ (1996) *J Mater Synth Proc* 4:127
32. Duque NB, Malgarejo ZH, Suárez OM (2005) *Mater Charact* 55:167
33. Mishnaevsky LL Jr (2006) *Compos Sci Technol* 66:1873
34. Nardone VC, Strife JR, Prewo KM (1991) *Mater Sci Eng A* 144:267

35. Pandey AB, Majumdar BS, Miracle DB (1999) Mater Sci Eng A 259:296
36. Qin S, Zhang G (2000) Mater Sci Eng A 279:231
37. Khalili S (2006) A study on the fracture behavior of Al6061-Al6061/SiC<sub>p</sub> composite produced by powder extrusion method. MSc thesis, Sharif University of Technology, Tehran
38. Nouri A (2005) Fabrication of Al/Al-SiC<sub>p</sub> composite via extrusion and evaluation of its fracture behavior. MSc thesis, Sharif University of Technology, Tehran
39. ASTM E8m-00b standard test method for tension testing of metallic materials. Annual Book of ASTM Standards, Philadelphia
40. ASTM E399-90 (Reapproved 1997) standard test method for plane-strain fracture toughness of metallic materials. Annual Book of ASTM Standards, Philadelphia
41. ASTM E992-84 (Reapproved 1989) standard test method for determination of a fracture toughness of steels using equivalent energy methodology. Annual Book of ASTM Standards, Philadelphia
42. Nardone VC, Prewo KM (1986) Scr Metall 20:43
43. Smith CA (1990) In: Miracle DB, Donaldson SL (eds) ASM handbook: composites, 10th edn. ASM International, USA
44. O'Donnell G, Looney L (2002) Mater Sci Eng A 303:292
45. Miller WS, Humphreys FJ (1991) Scr Metall Mater 25:33
46. Ramakrishnan N (1996) Acta Mater 44:69
47. Liu DS, Manoharan M, Lewandowski JJ (1989) Metall Mater Trans A 20:2409
48. Osman TM, Lewandowski JJ (1996) Metall Mater Trans A 27:3937
49. Osman TM, Lewandowski JJ (1997) Mater Sci Eng A 229:1
50. Rice TM, Tracey DM (1969) J Mech Phys Solids 17:201